# Morphology dependent polymeric capillary optical resonator hydrostatic pressure sensor

**Marcelo A. Gouveia,[1,3,*] P. Duber Avila ,[1,2,3] Thiago H. R. Marques,[1] M. Cesar Torres[2] and Cristiano M. B. Cordeiro[1,4]**

[1] *Institute of Physics 'Gleb Wataghin', University of Campinas - UNICAMP, Brazil*
[2] *University Popular of Cesar, Colombia*
[3] *Equally contributing authors*
[4] *cmbc@ifi.unicamp.br*
[*] *alonsog@ifi.unicamp.br*

**Abstract:** A hydrostatic pressure sensor based on morphology dependent resonances in a polymeric tube is presented. By internal pressurization, normal tensions will increase the device's size and shrink its wall thickness, inducing a shift in the resonant wavelengths of the resonator. Numerical simulations indicate that there are two modal regimes of sensitivity and a maximum achievable sensitivity, related to the device's geometry, constitutive material and analysed mode order. A sensitivity as high as 0.36 ± 0.01 nm/bar has been experimentally found for a 1.8mm diameter PMMA tube with wall thickness of 80μm.



**OCIS codes:** (280.5475) Pressure measurement; (230.5750) Resonators;

## References and links

1. A. B. Matsko and V. S. Ilchenko, "Optical resonators with whispering-gallery modes-part I: basics," IEEE J. Sel. Top. Quantum Electron. **12**(1), 3–14 (2006).
2. V. S. Ilchenko and A. B. Matsko, "Optical resonators with whispering-gallery modes - Part II: Applications," IEEE J. Sel. Top. Quantum Electron. **12**(1), 15–32 (2006).
3. W. Liang, V. S. Ilchenko, A. A. Savchenkov, A. B. Matsko, D. Seidel, and L. Maleki, "Whispering-gallery-mode-resonator-based ultranarrow linewidth external-cavity semiconductor laser," Opt. Lett. **35**(16), 2822–2824 (2010).
4. H. Aouani, F. Deiss, J. Wenger, P. Ferrand, N. Sojic, and H. Rigneault, "Optical-fiber-microsphere for remote fluorescence correlation spectroscopy," Opt. Express **17**(21), 19085–19092 (2009).
5. T. Ling and L. J. Guo, "Analysis of the sensing properties of silica microtube resonator sensors," J. Opt. Soc. Am. B **26**(3), 471–477 (2009).
6. J. Wang, T. Zhan, G. Huang, P. K. Chu, and Y. Mei, "Optical microcavities with tubular geometry: properties and applications," Laser Photon. Rev. **8**(4), 521–547 (2014).
7. M. Sumetsky, "Whispering-gallery-bottle microcavities: the three-dimensional etalon," Opt. Lett. **29**(1), 8–10 (2004).
8. M. Sumetsky, Y. Dulashko, and R. S. Windeler, "Optical microbubble resonator," Opt. Lett. **35**(7), 898–900 (2010).
9. D. K. Armani, T. J. Kippenberg, S. M. Spillane, and K. J. Vahala, "Ultra-high-Q toroid microcavity on a chip," Nature **421**(6926), 925–928 (2003).
10. H. Kudo, R. Suzuki, and T. Tanabe, "Whispering gallery modes in hexagonal microcavities," Phys. Rev. A – At. Mol. Opt. Phys. **88**, 023807 (2013).
11. N. C. Frateschi and A. F. J. Levi, "Resonant modes and laser spectrum of microdisk lasers," Appl. Phys. Lett. **66**(22), 2932 (1995).
12. D. Van Thourhout and J. Roels, "Optomechanical device actuation through the optical gradient force," Nat. Photonics **4**(4), 211–217 (2010).
13. B. R. Johnson, "Theory of morphology-dependent resonances: shape resonances and width formulas," J. Opt. Soc. Am. A **10**(2), 343–352 (1993).
14. C. C. Lam, P. T. Leung, and K. Young, "Explicit asymptotic formulas for the positions, widths, and strengths of resonances in Mie scattering," J. Opt. Soc. Am. B **9**(9), 1585–1592 (1992).
15. R. Yang, A. Yun, Y. Zhang, and X. Pu, "Quantum theory of whispering gallery modes in a cylindrical optical microcavity," Optik (Stuttg.) **122**(10), 900–909 (2011).
16. J. C. Knight, G. Cheung, F. Jacques, and T. A. Birks, "Phase-matched excitation of whispering-gallery-mode resonances by a fiber taper," Opt. Lett. **22**(15), 1129–1131 (1997).

#231295 - $15.00 USD Received 26 Dec 2014; revised 19 Mar 2015; accepted 20 Mar 2015; published 16 Apr 2015

17. B. E. Little, J. P. Laine, and H. A. Haus, "Analytic theory of coupling from tapered fibers and half-blocks into microsphere resonators," J. Lightwave Technol. **17**(4), 704–715 (1999).
18. H. P. Wagner, H. Schmitzer, J. Lutti, P. Borri, and W. Langbein, "Effects of uniaxial pressure on polar whispering gallery modes in microspheres," J. Appl. Phys. **113**(24), 243101 (2013).
19. T. Weigel, C. Esen, G. Schweiger, and A. Ostendorf, "Whispering gallery mode pressure sensing," in *Proceedings of SPIE - The International Society for Optical Engineering*, **8439**, 84390T (2012)
20. M. Manzo, T. Ioppolo, U. K. Ayaz, V. Lapenna, and M. V. Ötügen, "A photonic wall pressure sensor for fluid mechanics applications," Rev. Sci. Instrum. **83**(10), 105003 (2012).
21. T. Ioppolo and M. V. Ötügen, "Pressure tuning of whispering gallery mode resonators," J. Opt. Soc. Am. B **24**(10), 2721–2726 (2007).
22. S. Timoshenko and J. N. Goodier, *Theory of Elasticity*, (McGraw-Hill, 1969).
23. D. D. Wright, E. P. Lautenschlager, and J. L. Gilbert, "The effect of processing conditions on the properties of poly(methyl methacrylate) fibers," J. Biomed. Mater. Res. **63**(2), 152–160 (2002).
24. R. M. Waxler, D. Horowitz, and A. Feldman, "Optical and physical parameters of Plexiglas 55 and Lexan," Appl. Opt. **18**(1), 101–104 (1979).
25. M. van Eijkelenborg, M. Large, A. Argyros, J. Zagari, S. Manos, N. Issa, I. Bassett, S. Fleming, R. McPhedran, C. M. de Sterke, and N. A. Nicorovici, "Microstructured polymer optical fibre," Opt. Express **9**(7), 319–327 (2001).
26. S. C. Xue, R. I. Tanner, G. W. Barton, R. Lwin, M. C. J. Large, and L. Poladian, "Fabrication of microstructured optical fibers-part II: numerical modeling of steady-state draw process," J. Lightwave Technol. **23**(7), 2255–2266 (2005).
27. G. Senthil Murugan, M. N. Petrovich, Y. Jung, J. S. Wilkinson, and M. N. Zervas, "Hollow-bottle optical microresonators," Opt. Express **19**(21), 20773–20784 (2011).
28. M. J. Weber, *Handbook of Optical Materials* (The CRC Press, 2003)
29. P. Wang, M. Ding, T. Lee, G. Senthil Murugan, L. Bo, Y. Semenova, Q. Wu, D. Hewak, G. Brambilla, and G. Farrell, "Packaged chalcogenide microsphere resonator with high Q-factor," Appl. Phys. Lett. **102**(13), 131110 (2013).
30. W. C. Oliver and G. M. Pharr, "An improved technique for determining hardness and elastic modulus using load and displacement sensing indentation experiments," J. Mater. Res. **7**(06), 1564–1583 (1992).

## 1. Introduction

Whispering-Gallery Mode (WGM) based devices have found application in a wide range of fields, from which can be cited laser cavity, spectroscopy, sensing and filters, amongst others [1–6]. The geometry of such devices is generally spherical or cylindrical, although other geometries such as bottles [7], bubbles [8], toroids [9] and more complex structures [10] have been successfully introduced which have found interesting applications in specific areas. As an example, micro disks were suggested for studying nonlinear effects [11] and, more recently, optomechanical interactions [12].

Great efforts have been directed to this class of photonic devices in order to understand its field dynamics and inherent effects, such as its morphological dependency, its leaky character, and further manipulation of the resonant fields. The studies carried out by B. R. Johnson, Lam et al. and Yang et al. clarify in detail the phenomenological interpretation and fundamental concepts of WGMs in spherical and cylindrical resonators [13–15].

Likewise, it is important to note the contributions given by Knight et al. and Little et al. describing the theory of excitation of WGMs through tapered fibers [16,17], a method that enhanced the power coupling efficiency up to 95% [2].

For sensing purposes, WGM based devices have been applied in many ways to measure environmental changes such as refractive index, chemical substances, and pressure [2,6,18–20]. The latter has been exploited in many different forms, such as for flow pressure measurement [20] or hydrostatic pressure [19]. Ioppolo and Ötügen have modelled and experimentally demonstrated the spectral behaviour of the resonant modes of a WGM resonator under an applied pressure [21].

This present article contributes to the analysis of cylindrical cavities by introducing a theoretical study and experimental confirmation of polymethylmethacrylate (PMMA) capillary resonators applied as a pressure sensor. Basically, the sensor will be internally pressurized and a specific spectral response is expected since it will be related to the device's morphology. To investigate such a response, we shall first introduce the elastic behaviour of the polymeric capillary when it is internally pressurized, the dependency of the refractive

#231295 - $15.00 USD Received 26 Dec 2014; revised 19 Mar 2015; accepted 20 Mar 2015; published 16 Apr 2015

index through the elasto-optic effect and the mode response to the stimulus. Next, the experimental analysis for capillaries with different geometries will be discussed, including the fabrication process and possible drawbacks inherent to the excitation method and data acquisition.

## 2. Theoretical model

The presence of resonant fields in curvilinear geometries introduces a powerful concept of photon confinement, as it is not compulsory to have a well-defined refractive index step design, which is, *au contraire*, needed in Fabry-Perot based cavities, for instance. Such confinement, though, comes with a fundamental condition of scattering, which is clearly observed when Maxwell's equations are rearranged in such a way that allows comparison with Schrodinger's equation [13,15]. In cylindrical coordinates, {ρ, φ, z}, by a suitable change of variables, Maxwell's equation for a $TM^z$ leads to a Schrodinger-like equation, as follows [15],

$$\begin{cases} -\dfrac{d^2\tilde{E}_z(\rho,k_0)}{d\rho^2} + V_{TM}^m(\rho,k_0)\tilde{E}_z(\rho,k_0) = \Pi\tilde{E}_z(\rho,k_0), \\ E_z(\rho,k_0) = \dfrac{\tilde{E}_z(\rho,k_0)}{\sqrt{\rho}} \end{cases} \tag{1}$$

where $m$ is the azimuthal mode order number; $V_{TM}^m(\rho,k_0) = U_{TM}(\rho,k_0) + (4m^2-1)/4\rho^2$, which can be interpreted as an effective potential with applied potential $U_{TM}(\rho,k_0) = k_0^2\left[1-n^2(\rho)\right]$. The term $n(\rho)$ stands for the refractive index of the capillary, evaluated with $n_1 = 1.48$ inside the capillary wall, defined as $a \equiv \rho_{out} - \rho_{int}$, or $\rho_{int} < \rho < \rho_{out}$, where $\rho_{int}$ and $\rho_{out}$ are the inner and outer capillary radii - as depicted in Fig. 1(a) -, and $n_2$ elsewhere and $\Pi \equiv k_0^2$, being the system eigen energy, where $k_0 \equiv 2\pi/\lambda_0$ the wave vector, with $\lambda_0$ being the associated wavelength. $\tilde{E}_z(\rho,k_0)$ is the scalar function for $TM^z$ mode and is represented by a suitable set of Bessel functions and Bessel-related functions. Its continuity over the entire space is taken implicitly by Eq. (1) and the following continuity conditions derived from Maxwell's equations: $n(\rho)E_z(\rho,k_0)$ and $[1/n(\rho)]dE_z(\rho,\varphi)/d\rho$. The derivation of the $TE^z$ mode equation is similar to the above mentioned despite on boundary of the guide, where the effective potential $V_{TE}^m(\rho,k_0)$ diverges from $V_{TM}^m(\rho,k_0)$ by $2/\mathrm{n}(\rho)\left[\mathrm{dn}(\rho)/\mathrm{d}\rho\right]\left[\mathrm{d}/\mathrm{d}\rho\right]$, in modulus [15].

From the point of view of Eq. (1) as a Schrodinger-like equation, the existence of surface modes (SMs) emerges naturally, as the azimuthal correction $-(4m^2-1)4\rho^2$ - brings a geometrical, and fundamental, condition of confinement by which the wave is bound not just by a positive refractive index contrast - as it should be in Cartesian coordinates - but also by the geometry and the mode azimuthal correction as well. In this way, the wave could cease its harmonic form and exhibit an evanescent form even inside the waveguide. Because of such a condition, solid rods, spheres or any other curvilinear devices are capable of supporting a resonant field. Such superficial modes are the so-called Whispering Gallery Modes (WGMs). For capillaries - and other hollow devices - a second kind of mode is present as well, which is closely related to the wall thickness or, in other words, the Cartesian definition of bound waves. For such modes, named in this article as bulk modes (BMs), the confinement condition, as expected, is defined by both the inner and outer surfaces of the capillary, $\rho_{int}$ and $\rho_{out}$, rather than the azimuthal correction: $(4m^2 - 1)/4\rho^2$. Figure 1(b) presents both $TM^z$ modes: surface and bulk, found in such devices. As usual in Quantum Mechanics, all state turning points are obtained by equalling the state energy, $\Pi$, to the effective potential, $V_{TM}^m(\rho,k_0)$.

#231295 - $15.00 USD Received 26 Dec 2014; revised 19 Mar 2015; accepted 20 Mar 2015; published 16 Apr 2015

Doing so for $k_0^2 = V_{TM}^m(\rho, k_0)$, it will lead to a set of three turning points $\{\rho_1, \rho_2, \rho_3\}$, as seen in Fig. 1(b). The first two points, $\{\rho_1, \rho_2\}$, delimit the bound state region, or the confined resonant field. Note that in SMs, the first turning point lies inside the wall, squeezing the mode against the external wall interface as long as $m$ is increased. The third turning point, $\rho_3$, brings the fundamental scattering condition to the device, where even a strongly confined mode has probability to couples to the vacuum, implying in curvature losses, since the azimuthal correction, $(4m^2 - 1)/4\rho^2$, vanishes for greater values of radial distance. For simplicity, the discussion of fundamental losses will be avoided, as this study just aims the resonant wavelength dependency on the internally applied pressure in a capillary resonator. Discussions in depth of curvature losses is found in [11] and its references.

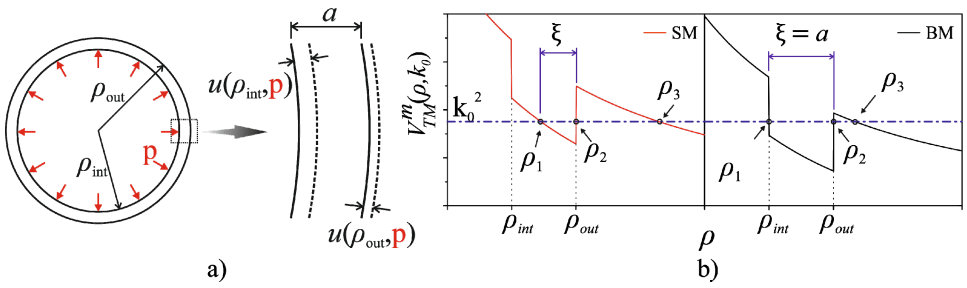


Fig. 1. a) Capillary describing the inner and outer radii - $\rho_{int}$ and $\rho_{out}$ -, the pressure applied, $p$ - and its morphology response. b) Effective potential and turning points of surface modes SM, and bulk modes BM. The parameter $\xi$ lies as the distance between the first two turning points, $\rho_1$ and $\rho_2$.

By experiencing changes in the internal pressure, the effective potential shifts according to the applied strain over the wall, which yields both shape and refractive index change. The displacement, $u(\rho,p)$, of a point with radial position $\rho$, inside the wall, for an applied internal pressure - $p$ -, according to the Hooke law, in the plane stress approach, is given by [22]

$$u(\rho,p) = \rho.\left[\frac{\rho_{int}^{\,2}}{\left(\rho_{out}^{\,2} - \rho_{int}^{\,2}\right)}\right].\left[(1-\upsilon) + (1+\upsilon)\left(\frac{\rho_{out}}{\rho}\right)^2\right].\frac{p}{E}, \tag{2}$$

where the influence of the chosen material took place as the Young's modulus, $E$, and the Poisson's ratio, $v$. For PMMA capillaries, the value of the these parameters are, respectively, $2.2 \times 10^4$ bar (2.2GPa) and 0.37 [23]. The dynamics of both inner and outer radii, defined from Eq. (2) are,

$$\begin{cases} \rho_{int}(p) = \rho_{int} + u(\rho_{int}, p) \\ \rho_{out}(p) = \rho_{out} + u(\rho_{out}, p) \end{cases}, \tag{3}$$

as depicted in Fig. 1(a).

The elasto-optic effect is proportional to the applied strain and, in the case of an internal pressurization, must have higher influence on the inner radius as $u(\rho_{int},p) > u(\rho_{out},p)$ and equalling to the bulk at the outer radius, where is found under environment pressure. For a weak approximation in plane stress approach, the following expression models such effect,

$$n(\rho,p) = n_1 + \frac{n_1^3}{2}\left[\frac{(c_{11}+c_{12})(1-\upsilon)}{2E}\right]\left(\frac{\rho_{out}-\rho}{\rho_{out}-\rho_{int}}\right)^2\left(\frac{\rho_{int}}{\rho}\right)^2 p, \tag{4}$$

where $c_{11}$ and $c_{12}$ are the elasto-optic coefficients, being 0.3 and 0.297, respectively [24], and $n_1 = 1.48$, for PMMA. From the averaged value of Eq. (4),

#231295 - $15.00 USD Received 26 Dec 2014; revised 19 Mar 2015; accepted 20 Mar 2015; published 16 Apr 2015

$$\left\langle n(\rho,p)-n_1\right\rangle=\left[\frac{\left(\frac{\rho_{out}}{\rho_{int}}\right)^2-2\left(\frac{\rho_{out}}{\rho_{int}}\right)\ln\left(\frac{\rho_{out}}{\rho_{int}}\right)-1}{\left(\frac{\rho_{out}}{\rho_{int}}-1\right)^3}\right]p\left(1.4\times10^{-6}\right), \qquad (5)$$

where $\langle n(\rho,p) - n_1\rangle \rightarrow p.(4.7 \times 10^{-7})$, when $\rho_{int} \rightarrow \rho_{out}$. Therefore, in practical conditions, the elasto-optic effect may be considered as a secondary effect, yielding that the resonant dependency might be purely morphological, since it would be necessary higher pressure ($p \gg$ 10 bar) applied in a very thin capillary, and in such a condition, the device is likely being blown up before any perceptible wavelength motion due to the elasto-optic effect.

From a heuristic approach, the normalized infinitesimal resonant wavelength deviation would vary according to the normalized mode confinement, $\xi$ (see Fig. 1(b)), and resonant radial position shift, $\langle\rho\rangle$, or explicitly, $\delta\lambda/\lambda = \delta\xi/\xi + \delta\langle\rho\rangle/\langle\rho\rangle$ . The mode confinement can be defined roughly as the distance between the two turning points, $\xi \equiv \rho_2 - \rho_1$, and the radial position as $\rho=\int_{\rho_1}^{\rho_2}\rho d\rho\left|\tilde{E}_z(\rho,k_0)\right|^2$ [15]. Such expression has a limit when $\rho_1$ tends to $\rho_2 = \rho_{out}$, of which will lead to a closed expression, since, when $\rho_1 \rightarrow \rho_{out}$, $\delta\xi \rightarrow 0$ and $\langle\rho\rangle \rightarrow \rho_{out}$. Therefore, $\delta\lambda/\lambda \approx \delta\rho_{out}/\rho_{out}$ and, substituting (3) into, it yields,

$$S\equiv\frac{\Delta\lambda}{\Delta p}=\frac{2\lambda_0}{E}\left[\left(\frac{\gamma}{2-\gamma}\right)^2-1\right]^{-1}, \qquad (6)$$

where the dimensionless parameter $\gamma$ is defined as the ratio of the outer diameter, $D = 2\rho_{out}$ and wall thickness, $a$ – $\gamma \equiv D/a$ - and shall be considered as a fundamental geometrical parameter from here so on. Note that the equation found approaches asymptotically to $S_\infty = \lambda_0(\gamma-3)/2E$.

In addition, Eq. (6) lies as a morphological limitation over the achievable sensitivity. Analysing such infinitesimal displacement for BMs, the distance between the two turning points becomes the wall thickness, $\xi \rightarrow a$, and, as an implication of the elastic behaviour, $\delta\xi = \delta a = u(\rho_{out},p) - u(\rho_{int},p) < 0$. Such result is expected by analogy to a quantum well, where the eigen energy, $\Pi$, depends on the inverse of the square well length, $\Pi \propto a^{-2}$, leading to a blue shift in the resonant wavelength. In that case, the sensitivity will, by definition, be lower than the one found in SMs, which is already asymptotically limited by Eq. (6).

In order to calculate the resonant wavelength shift as function of the applied pressure, it is just necessary to include the moving radii positions for an applied pressure, expressed in Eqs. (2) and (3), in the two continuity condition already mentioned, evaluated at each turning point $\{\rho_1, \rho_2\}$, of which yield a four degrees of freedom homogeneous system. Solving numerically the its determinant for a given value of the azimuthal mode order number $m$, its roots should lead to a series of resonant wavelengths of the given effective potential $V_{TM}^m(\rho,k_0)$, where each resonant wavelength found can be indexed by two numbers, $(q,m)$, where $q$ represents the $qth$ resonant wavelength of a given order mode $m$. Alternatively, by fixing $k_0$ in a small spectral window, $q$ would vary implicitly due to the uniqueness condition of the solution. Figure 2 depicts the numerical sensitivity data obtained for a series of values of $\gamma$ for SMs and BMs (location in the effective potential indicated in the inset) at wavelengths near 1.5μm, which are also listed in the table beside the Fig. 2. The numerical simulation indicated that SMs might have sensitivity as high as the one given by Eq. (6) and BMs should have their

#231295 - $15.00 USD Received 26 Dec 2014; revised 19 Mar 2015; accepted 20 Mar 2015; published 16 Apr 2015

associated sensitivities scattered just below the curve, increasing with the azimuthal mode order number *m*.

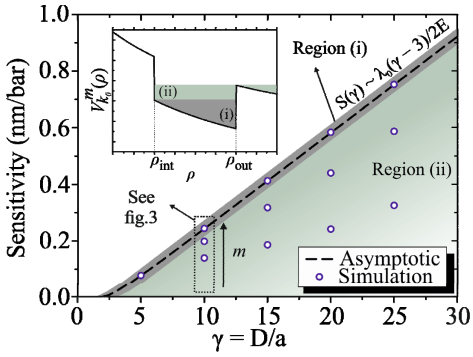


| Numerical Sensitivity | | |
|---|---|---|
| γ | *m* | *S (nm/bar)* |
| 5 | 2400 | 0.06 |
| | 2700 | 0.07 |
| 10 | 4500 | 0.14 |
| | 4700 | 0.20 |
| | 6200 | 0.24 |
| 15 | 3200 | 0.18 |
| | 3800 | 0.32 |
| | 4200 | 0.41 |
| 20 | 2200 | 0.24 |
| | 2700 | 0.44 |
| | 3000 | 0.58 |
| 25 | 3400 | 0.32 |
| | 4000 | 0.59 |
| | 4500 | 0.75 |

Fig. 2. Sensitivity dependence of resonant modes near 1500 nm of capillaries resonators surrounded by air for surface modes (i) and bulk modes (ii). Numerical data are listed in embedded table.

The sensitivity dependency on the mode number *m* were investigated, where a resonator with $\gamma = 10$ (D = 2mm and $a = 0.2$mm) had its resonant modes simulated for various values of *m*, as shown in Fig. 3. The model states that the azimuthal mode order should play an important role in the sensitivity of bulk modes, as its values scale with *m*. However, the values found for SMs fluctuated around the analytical one, evaluated with Eq. (6), $S(\gamma = 10) = 0.242$ nm/bar, with $\lambda_0 = 1.5\mu$m. Such fluctuation could be explained by the resonant field form and its contribution to the sensitivity, since the mode radius $\langle\rho\rangle$ depends directly on its shape.

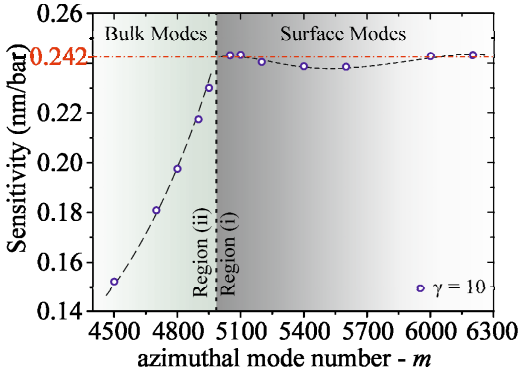


Fig. 3. Sensitivity as function of the azimuthal mode number - *m* - for a capillary resonator with geometrical parameter $\gamma = 10$ (D = 2mm and a = 0.2mm).

## 3. Sensor fabrication and experimental analysis

The chosen method for suitably obtaining samples for pressure sensing is based on drawing of PMMA's capillaries preforms through a polymer optical fiber drawing tower. Important geometrical parameters such as external diameter and wall thickness can be monitored and tuned directly by changing the furnace temperature, feed and pulling velocities and internally applied pressure [25].

Capillary preforms with external diameter of few millimetres and dimensionless parameter $\gamma \equiv D/a \approx 7.7$ were pulled at 210°C with tension of 60g. With these parameters, a standard diameter deviation of 1.8% through a 15m long capillary was measured and the levels of partial hole collapse were kept bellow 10%. The hole deformation, in this case, is influenced

#231295 - $15.00 USD Received 26 Dec 2014; revised 19 Mar 2015; accepted 20 Mar 2015; published 16 Apr 2015

mainly due to the polymer surface tension [26]. Since a single capillary is being fabricated instead of a complex structure with adjacent holes - such as microstructured polymeric optical fibres -, there is no deformation due to the existence of adjacent holes and the partial hole collapse is minimized. Then, by varying the internal pressure and pulling velocity during the drawing, a variety of suitably samples was produced from this method, covering a wide range of outer diameter from about few hundreds of micrometres to 3 millimetres, and $\gamma$ spanning from 2 to 25. A 4 × optical microscopy of a typical capillary is shown in Fig. 4(a). The typical value of the quality factor, Q-Factor, found for all produced PMMA capillaries with sub millimetric outer diameter is about $10^4$. It is a poor value compared to other structures such as microspheres and bottles produced in silica ($Q < 10^8$) [1,27]. Such low value is due, fundamentally, to scattering induced by internal and external surface roughness and intrinsic material absorption at working range wavelengths - around 1.5 μm [6].

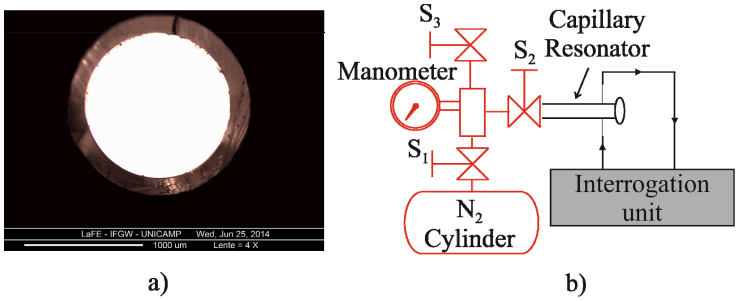


Fig. 4. a) A 4x optical microscopy of a typical capillary WGR used during the investigation. b) Diagram of the experimental apparatus used to investigate the device.

Furthermore, the fabrication process limits the theoretical achievable sensitivity, as it is difficult to obtain reliable samples with wall as thin as 30μm, below which the fiber has its toughness strongly affected. In addition, the measurable pressure range might decrease ($\ll$10bar) by the fact that thinner walls would no longer support higher pressure, being broken under such condition.

A 2 μm thick silica fiber taper was used during all experiments to excite resonant modes in the capillary and collect the perturbed signal. The perpendicularly alignment of taper to the sample is essential to avoid possible coupling of helical modes in the capillary, maximizing the power exchange between the fiber taper fundamental mode and all phase-matched capillary resonant modes. An interrogation unit constituted by a tuneable laser system and a spectrometer with maximum resolution of 10 pm was used to launch an input signal and analyse the output signal coming from the sample via fiber taper.

The pressurization system designed to perform all try-outs is depicted in Fig. 4(b). A pressure cell connected to a Nitrogen cylinder was used in order to control efficiently the capillary pressure. All experiments were performed in depressurization regime, because of better control over the applied pressure values. Figures 5(a) and (b) present, respectively, the resonant output sensitive for internal pressurization and three resonance displacement of three analysed samples with different values of $\gamma$, found in Table 1.

#231295 - $15.00 USD Received 26 Dec 2014; revised 19 Mar 2015; accepted 20 Mar 2015; published 16 Apr 2015

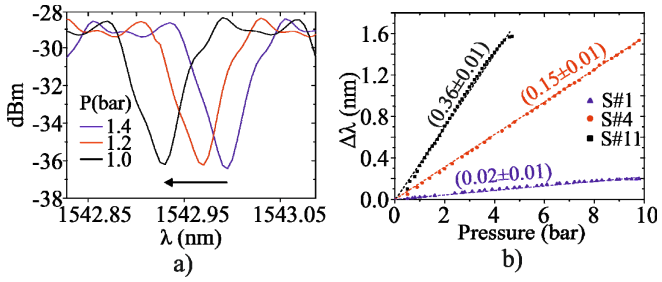


Fig. 5. a) Spectral output of a typical pressurized capillary resonator. b) Sensitivity range obtained experimentally.

The reported capillary sensors here present higher-pressure range (1-10 bar) than those found in [19–21] where the applied pressure is in the mbar regime. Their sensitivity [19,20], however, is far greater than the reported values in this letter mainly due the material choice with lower Young Modulus - PDMS and silicone instead of PMMA. On the other hand, the sensitivity achieved in PMMA's micro-sphere, (~0.2 nm/bar) [21], is agreement with those reported in this present study. As can be noted, therefore, the resonator's material indeed plays a fundamental role in the device sensitivity.

**Table 1. Experimental sensitivity of samples with different $\gamma$**

| # | $D$ (μm) | $a$ (μm) | $\gamma$ $D/a$ | $S$ (nm/bar) |
|---|---|---|---|---|
| **1** | 308 | 82.8 | 3.7 | 0.02 ± 0.01 |
| **2** | 711 | 58.9 | 12.1 | 0.15 ± 0.01 |
| **3** | 1888 | 146.1 | 12.9 | 0.16 ± 0.01 |
| **4** | 688 | 57.1 | 12.0 | 0.16 ± 0.01 |
| **5** | 2161 | 157.5 | 13.7 | 0.17 ± 0.01 |
| **6** | 2337 | 178.0 | 13.1 | 0.19 ± 0.01 |
| **7** | 2624 | 193.0 | 13.6 | 0.21 ± 0.01 |
| **8** | 1367 | 91.5 | 14.9 | 0.28 ± 0.01 |
| **9** | 1638 | 85.2 | 19.2 | 0.30 ± 0.01 |
| **10** | 1370 | 59.0 | 23.2 | 0.32 ± 0.01 |
| **11** | 1826 | 79.9 | 22.8 | 0.36 ± 0.01 |

The hypothesis that the sensitivity, despite the Young's modulus and mode order, should increase as function of the geometrical parameter $\gamma$, is experimentally supported as could be noticed in Table 1, where it is found all data from all samples analysed, and depicted in Fig. 6(a). Possible fluctuations could be found, as the sensitivity depends on other physical parameters as well, such as the order mode and Young's Modulus, in which could be seen at samples #2, #3 and #4 in the Table 1. Moreover, the reproducibility was investigated using the sample #11. As could be seen in Fig. 6(b) and its inset, the sample was tested three times consecutively, and was found a slight modification on the sensitivity, (0.01nm/bar), of which is inside the device's deviation. It suggests that the morphology dependence of all geometrical attributes should be under elastic regime for the applied pressure range in question, rather than in a plastic regime, where structural deformations are likely to happen, evolving to a spectral accumulated hysteresis after several measurement attempts.

Furthermore, as the pressure measurements usually do not exceed 10 minutes, thermal variations are not taken into account, and were not observed, since no hysteresis were noticed,

#231295 - $15.00 USD Received 26 Dec 2014; revised 19 Mar 2015; accepted 20 Mar 2015; published 16 Apr 2015

although for longer measurements it is indeed necessary to be aware of possible temperature-induced wavelength displacement. As an example, in the limit case for a tight confined surface mode, the device's thermal sensitivity is given as $S_T \approx \lambda_0(\alpha_T + \beta_T)$, where $\alpha_T \approx 5.05 \times 10^{-5}$ K$^{-1}$ and $\beta_T \approx -1 \times 10^{-4}$ K$^{-1}$ [28] are the PMMA's linear expansion and bulk refractive index thermal coefficients, respectively. At $\lambda_0 = 1.55\mu$m, the theoretical thermal sensitivity is around −0.05 nm/K, which clearly would become an issue, implying in considerably fluctuations over the spectral for long-time measurements.

The fundamental limitation of the sensitivity pointed out in the theory still holds, as all experimental sensitivity data lies under the Eq. (6), even for Young's modulus of 3.1GPa (about the maximum achieved in the literature for PMMA [23]). Moreover, note that as long as $\gamma$ increases, the deviation to the theoretical one rises. In fact, this effect may occur due to an eventual mismatching between the fundamental mode in the fiber taper and resonator's lower order modes [16,17,29], since each component (taper fiber and capillary) is made of different material with different refractive index - silica and PMMA. As reported in the literature, the selectiveness of resonant modes is closely related to the phase-matching and overlap of those with the fundamental mode of the fiber taper used [16,17]. Wang et al. concluded that, for high refractive index microsphere excited from 2 μm thick tapered SMF fiber, the phase-matching benefits higher order resonant modes and this property can be tuned by changing the surrounding medium, resulting that the fundamental mode travelling through the fiber taper would increase its effective index, as well as the microsphere would have some higher order modes suppressed from the output spectrum, as their resonant conditions are no longer satisfied [29]. Hence, the taper dimensions and the surrounding medium - together the capillary's material and geometry - plays an important role to achieve higher sensitivity in the present device as well.

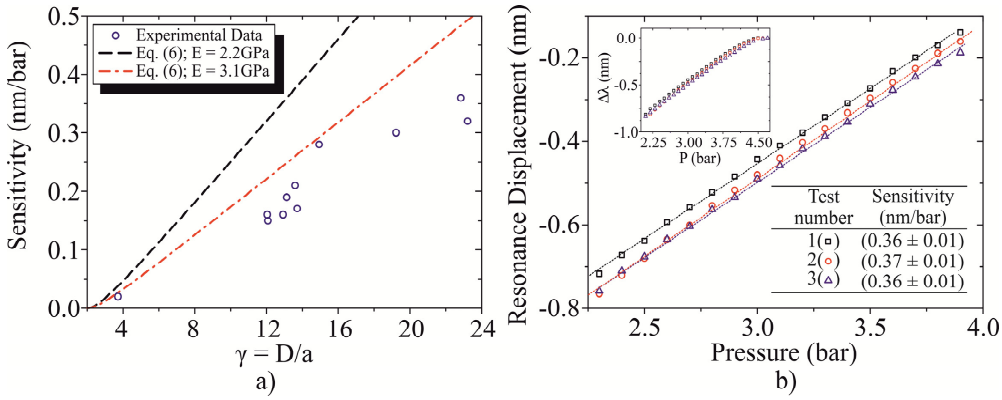


Fig. 6. a) Dependence of the sensitivity as function of $\gamma$, of all samples listed in Table 1, compared with the analytical sensitivity (Eq. (6)) for two values of Young's modulus (2.2 and 3.1GPa). b) Fitting of the reproducibility (at the inset) of consecutive measurements for the sample 11. Note that no hysteresis has been observed through the try-out, as indicated by each sensitivity value found at each test.

The effective range of pressure measurements should be limited a priori by the rupture modulus of the PMMA, (0.7- 2.0) × $10^3$ bar [23]. The wall thickness and the process of closure the capillary end, however, should decrease greatly this number. In fact, some samples have been tested until break, which usually happened around 10 to 15 bar, decreasing for capillary with thinner wall. Such issue can be overcome by fabricating greater resonators, with bigger wall's size, while maintaining higher values of $\gamma$. The bigger the resonator, however, the greater the mode density and the Q-factor, being necessary higher resolution (<10pm) optical characterization setup.

#231295 - $15.00 USD Received 26 Dec 2014; revised 19 Mar 2015; accepted 20 Mar 2015; published 16 Apr 2015

By employing other constitutive material, such as silica, it may improve the modal selectivity, since both fiber taper and capillary would be made by the same material. Worse sensitivity, however, must be expect, as silica has Young's modulus far greater than PMMA's one (about 73GPa, which yields 33 times greater than PMMA's one) [30], since the sensitivity is proportional to the inverse of the Young's Modulus. In the practical point of view, with such high Young modulus, the motion of the resonant wavelength would just be perceptible whether high pressure is applied, leading to a pressure insensitive device.

This new pressure sensing approach can be applied to in-line multi-resonators for higher dynamic range pressure measurements. In this situation, distinct regions of the capillary can be processed to have different $\gamma$ parameter, spanning the operational range of sensitivity and applied pressure. This potential multiplexing capability is not easily performed with other resonators devices reported in literature [19–21].

## 4. Conclusion

We have studied and demonstrated a pressure sensor based on the morphology dependent resonant modes of an internally-pressurized PMMA capillary. A theoretical model was described and analysed, showing two sensitivity regimes: for surface modes (SMs) and bulk modes (BMs) that interact with both the internal and external surfaces. The fundamental sensitivity upper limit was found to depend on the material's Young's modulus, resonant wavelength and the ratio of the outer diameter to wall thickness, $\gamma$. Numerical simulations indicate that SMs can offer sensitivities as high as the fundamental value and BMs would be less sensitive due to the wall width shrinkage and modal position within the capillary wall.

Experimental results indicate that the device sensitivity indeed increases with increasing $\gamma$. A sensitivity as high as (0.36 ± 0.01) nm/bar was found for a capillary with $\gamma$ = 22. The resonant mode excitation might be considered as well, since its order would influence directly the achievable sensitivity.

Further studies are being directed to better understand the role of the phase-matching between the fiber taper mode and the capillary WGMs, as changing the geometry of the tapered fiber would change its fundamental mode’s propagation constant as well, thus permitting some engineering of the capillary modes spectra for better achievable sensitivity. Inherent to the powerful simplicity of the present device, it could be post processed in order to perform as an in-line multi resonator array, spanning the pressure and sensitivity range greatly.

## Acknowledgment

This study received financial support by FINEP (under project 0112039300), CNPq and FAPESP. Duber Avila acknowledges University Popular of Cesar for their support in the development of staying during the investigation. Marcelo Gouveia acknowledges CNPq for his scholarship.

The authors are grateful to Prof. Dr. José A. Roversi for illuminating advice on the simulation in the Quantum Mechanics picture and all group members of the Special Fibre Laboratory (LaFE) for thoughtful discussions.

#231295 - $15.00 USD Received 26 Dec 2014; revised 19 Mar 2015; accepted 20 Mar 2015; published 16 Apr 2015